RSC Advances

This is an *Accepted Manuscript*, which has been through the Royal Society of Chemistry peer review process and has been accepted for publication.

Accepted Manuscripts are published online shortly after acceptance, before technical editing, formatting and proof reading. Using this free service, authors can make their results available to the community, in citable form, before we publish the edited article. This *Accepted Manuscript* will be replaced by the edited, formatted and paginated article as soon as this is available.

You can find more information about *Accepted Manuscripts* in the Information for Authors.

Please note that technical editing may introduce minor changes to the text and/or graphics, which may alter content. The journal's standard Terms & Conditions and the Ethical guidelines still apply. In no event shall the Royal Society of Chemistry be held responsible for any errors or omissions in this *Accepted Manuscript* or any consequences arising from the use of any information it contains.

ROYAL SOCIETY OF CHEMISTRY

www.rsc.org/advances

First-principles prediction on Graphene/SnO_2 heterostructure as a promising candidate for FET

Run-wu Zhang, Chang-wen Zhang, Hang-xing Luan, Wei-xiao Ji, and Pei-ji Wang*

School of Physics and Technology, University of Jinan, Jinan, Shandong，250022, People's Republic of China

ABSTRACT

Very recently, the graphene/SnO_2 heterostructures (G/SnO_2 HTSs) were successfully synthesized experimentally. Motivated by this work, the adhesion and electronic properties of G/SnO_2 HTSs have been studied by using first-principles calculations. It is found that the graphene interacts overall with SnO_2 monolayer with a binding energy of -67~-70 meV per carbon atom, suggesting a weakly van der Waals interaction between graphene and SnO_2 substrate. Although the global band gap is zero, a sizable band gap of 10.2~12.6 meV at the Dirac point is obtained in all G/SnO_2 HTSs, mainly determined by the distortion of isolated graphene peeled from SnO_2 monolayer, independent on the SnO_2 substrate. When the bilayer graphene is deposited on SnO_2 substrate, however, a global gap of 100 meV is formed at the Fermi level, which is large enough for the gap opening at room temperature. Interestingly, the characteristics of Dirac cone with nearly linear band dispersion relation of graphene can be preserved, accompanied by a small electron effective mass, and thus the higher carrier mobility is expected. These finds provide a better understanding of the interfacial properties of G/SnO_2 HTSs and help to design the high-performance FET in nanoelectronics.

Keywords: First-principles calculation; Graphene; SnO_2; Band gap; FET

RSC Advances Accepted Manuscript

PACS: 73.22.-f, 71.15.-m

*Corresponding author: zhchwsd@163.com

TEL: ++86-531-82765976; FAX: ++86-531-82765976

I. Introduction

Graphene, a two-dimensional (2D) hexagon carbon network, has been attracted much attention since it has been synthesized in 2004 [1], and thus much efforts have been devoted its fundamental physics and the exploration of the possibility of application in electronic devices [2-6]. The unique behavior revealed in graphene is that the π and π* bands derived from C-p_z orbital disperse linearly to cross the Fermi level (E_F), and the electrons behave as massless Dirac fermions due to the equivalent two carbon sublattices [2,7]. Hence, graphene is expected to be used in the next-generation nanoscale electronic devices such as high-performance field effect transistors (FETs) operating at room temperature [8, 9]. However, the lack of band gap make it currently unsuitable for nanoelectronics, and thus opening and tailoring a band gap in graphene becomes one of the most important and urgent research topics.

To achieve graphene-based electronics devices, many approaches, such as cut 2D graphene into finite-sized 1D nanoribbons, [10] hydrogenation, [11] uniaxial strain, [12] and molecule doping [13], have been suggested to open an energy gap in graphene. The main disadvantage of these methods is that the carrier mobility and on-state current are greatly reduced because the destruction of honeycomb network introduces scattering centers, and enhances the carrier effective mass. Thus, the development of a reliable technique to create a finite gap without degrading the linear band dispersion character of graphene remains challenging. Recently, it is reported that the graphene/substrate HTSs [14-19] is easier to synthesize in experiments than the

RSC Advances Accepted Manuscript

aforementioned functionalized approaches. Especially, if the graphene/substrate interaction is weak, many intrinsic properties of monolayer graphene can be kept. Inspired by this result, more and more works have been performed to pursue an energy-gap without destroying the intrinsic properties of graphene. [17-19] Despite these achievements, the search for ideal substrates is still underway.

More recently, Miao [20] reported the geometric stability and lithium storage performance in new constructed G/SnO_2 HTS. They predict the stable interface formed by C−O covalent bonds, which makes G/SnO_2 HTS more conductive than SnO_2. Paek [21] reported enhanced cyclic performance and lithium storage capacity of G/SnO_2 electrodes with 3D delaminated flexible structure. According to the TEM analysis, the graphene are homogeneously distributed on the loosely packed SnO_2 substrate in such a way that the nanoporous structure with a large amount of void spaces could be prepared. However, the electronic properties of G/SnO_2 HTS have not been investigated up to date. Motivated by this experiment, we explore the energetics and electronic properties of G/ SnO_2 HTS and freestanding distorted graphene (FDG) peeled from SnO_2 substrate, as well as bilayer graphene (BLG) deposited on SnO_2 monolayer by using first-principles calculations. It is unexpected that, different from the previous reported G/semiconductor HTSs [14-20], no energy-gap opening is obtained in the G/SnO_2 HTS. However, the FDG peeled from G/SnO_2 HTS opens a sizeable energy gap (10.2~12.3 meV) with the linear characteristic of graphene at the Dirac point. When the bilayer graphene is deposited on SnO_2 substrate, we also find a global gap of 100 meV at the Fermi level, larger than k_BT (26 meV) at room temperature, suggesting potential applications in graphene-based FET.

II. Computational method and details

All calculations are performed by means of the Vienna Ab Initio Simulation Package (VASP). [22,23] The electron-ion interactions were represented by the projector

RSC Advances Accepted Manuscript

augmented wave (PAW) potentials. [24] To treat exchange-correlation interaction of electrons, we chose the Perdew-Burke-Ernzerhof (PBE) functional within the generalized-gradient approximation (GGA). [25] To properly take into account the van der Waals (vdW) interactions in the layered structures, the DFT-D2 method [26,27] was used throughout all the calculations. The plane-wave basis set cutoff is 400 eV. The convergence thresholds for energy and force are 10^{-5} eV and 0.01 eV/Å, respectively.

To simulate G/SnO_2 HTSs, we considered an O-terminated surface of SnO_2 possessing a triangular lattice of O atoms at the topmost layer. The interface of G/SnO_2 HTS are simulated using a supercell model in which graphene is put on surface of SnO_2 monolayer, and a vacuum layer of 15 Å is used in the direction normal to SnO_2 monolayer. We imposed a commensurability condition between graphene and SnO_2, where a 4 × 4 lateral periodicity of graphene and 3 × 3 lateral periodicity of the SnO_2 monolayer are employed, as shown in Fig. 1. The small lattice mismatch between graphene and SnO_2 substrate is 2.5%.

III. Results and discussions

In this work, we consider three representative patterns of graphene on SnO_2 substrate: (i) a C atom of graphene on top of one of the Sn atoms (TS) (Figs. 1 (a)); (ii) a C atom of graphene on top of one of the O atoms (TO) (Figs.1 (b)); (iii) a C atom of graphene on top of bridge site between Sn and O atoms (B) (Figs. 1 (c)). After structural relaxations, we find that the graphene keeps its original planar and hexagonal atomic network, while maintaining the interlayer spacing of ~ 3.0 Å (Table 1), when bonded to the SnO_2 monolayer. Notice that the interlayer spacing is much larger than the sum of covalent radii of C and oxygen atoms, suggesting that the interfacial C-O lengths of G/SnO_2 HTSs are beyond the bonding range. In addition, we also find that the corrugation of the graphene layer is ~ 0.07 Å, close to that in G/MoS_2 [16] and G/SiC HTSs [28].

RSC Advances Accepted Manuscript

To quantitatively characterize the interface interactions, the binding energy (E_b) between the graphene and SnO_2 monolayer is calculated as

$$E_b = E(G/SnO_2) - E(G) - E(SnO_2) ,$$

where $E(G/SnO_2)$, $E(G)$, and $E(SnO_2)$ are energies of G/SnO_2 HTS, isolated graphene and SnO_2 monolayer, respectively. Fig. 2 displays the E_b per C atom with respect to the spacing between graphene and SnO_2 for TS, TO, B patterns, respectively. At the optimized interlayer spacing, the E_b in three patterns is about -67~ -70 meV (Table I), demonstrating that the E_b is not sensitive to the adsorption patterns. These can be understood through a comparison with the adsorption of graphene on HfO_2 surfaces [29]. In the case of HfO_2 substrate (-112meV/C), it is found that the absorption of graphene is caused mainly by the hybridization between the C-π and O-2p states with Hf-d character. By contrast, the present results suggest the graphene is bound to SnO_2 via the weakly vdW mechanism. Since the energy of pattern B is lowed by about 3 meV than that in patterns TO and TS, we only consider pattern B in the following.

To check the validity of vdW interactions to G/SnO_2 HTS, We also calculated the interlayer distance dependence of the E_b per C atom of G/SnO_2 HTSs using PBE approximation, as shown in Table I. A comparison study shows that the variational trends and equilibrium interlayer spacings given by PBE+vdW and PBE approaches are different significantly for all stacking patterns. The resulting interlayer spacing are ~3.6 Å for TS, TO, and B patterns without vdW interactions, and the corresponding E_b are ~ −11~−16 meV. Obviously, there is a significant difference between the results with and without inclusion of the vdW interactions, indicating that the vdW interaction is extremely important for accurately describing the geometric structure of the G/SnO_2 HTS.

To explore whether the electronic structures of graphene can be affected by SnO_2 substrate, we examine the band structures of the G/SnO_2 HTSs, as shown in Figs. 3(a-c). As a comparison, the band structures of free-standing graphene and SnO_2

RSC Advances Accepted Manuscript

monolayer are shown in Figs. 3(d) and (e), respectively. For the SnO_2 monolayer, Eg = 2.75 eV, consistent with the previous results. [30] Due to the relatively weak interaction between graphene and SnO_2 monolayer, a size band gas of 13.4 meV, 15.8 meV, and 17.2 meV for patterns TO, TS, B, respectively, are obtained. However, the hybridized graphene π and π* bands with oxygen atoms significantly cross E_F and thus unexpected metallic behavior appears for G/SnO_2 HTSs, in contradiction to the previous results reported for G/semiconductor HTSs [14-19]. The possible reason can be attributed to the interlayer-induced self-doping phenomenon, as found in G/BC_3 HTS [31], which significantly reduces the gap for the whole band structure and renders graphene *n* or *p*-type metallic behaviors. In fact, these results are in good agreement with experimental observations, in which G/SnO_2 HTS has a higher electric conductivity [20, 21].

To further explain this unexpected phenomenon, we display the partial density of states (PDOSs), as shown in Fig. 3(f). One can see that the E_F cross the Sn-5s and O-2p states at the conduction band minimum (CBM), as well as C-2p states at the valance band maximum (VBM). This is because that the C-2p states of graphene lose some electrons, making E_F shift down clearly, while the CBM from Sn-5s and O-2p hybridized states make the E_F move up correspondingly due to the electrons transfer from graphene to SnO_2 monolayer. Also, further Bader charge analysis indicates that the charge density is redistributed by forming electron-rich and hole-rich regions between graphene and the SnO_2 monolayer, as shown in Fig. 4 (a) According to π-electron tight-binding (TB) model [32] of bipartite lattices, the dispersion relation near E_F can be expressed as [33,34]

$$|E(k)| = \pm\sqrt{\Delta^2 + (\hbar \upsilon_F k)^2} \quad (2)$$

Here, k is the wave vector relative to the K point, v_F is the Fermi velocity, and Δ is the onsite energy difference between two sublattices. For free-standing graphene, the onsite energies of A and B sublattices are identical (Δ = 0), and thus results in the

RSC Advances Accepted Manuscript

Dirac-like linear dispersion relation. When graphene is deposited on SnO_2 substrate, the symmetry-breaking substrate potential is introduced, and thus the inversion symmetry of graphene is broken by making $\Delta \neq 0$, giving rise to a nonzero band gap, $E_g = 2\Delta$. As is shown in Figs. 4 (a) and (b), the charge transfer from graphene to SnO_2 monolayer and non-uniformity of electron charges disrupt the degeneracy of the π and π* bands at K point, resulting in the band gap opening.

It is the weakly interaction between graphene and SnO_2 monolayer that FDG can be easily peel from G/SnO_2 HTS, as shown in Fig. 1(d). The structure of FDG is the same as that of G/SnO_2 HTS except that the substrate is removed to distill the effect of the structure distortion on the band structure. The equivalence of the two carbon sublattices inside FDG lattice basically remains unaffected because of the slightly corrugation of carbon atoms, so the geometric structure of the FDG is almost the same as the silicene or germanene [35, 36]. Fig. 5 further displays the band structures of the FDG in patterns TO, TS, B, respectively. Interestingly, one can see that the π and π* bands repulse each other, forming a direct band gap at the K points. The calculated band gap is about 10.2, 12.3, and 10.6meV for patterns TO, TS, B, respectively. These gap values are comparable to those obtained for graphene on hydroxylated (0001) surfaces of SiO_2 [37], smaller than that of hexagonal BN surface [38], indicating that the transport properties of FDG decreases slightly compared with the pristine graphene.[37, 38] Remarkably, the curvature of the band dispersion around the Dirac point of FDG is almost linear, suggesting that the carrier effective mass and, consequently, the high carrier mobility are hardly influenced by SnO_2 substrate. It indicates that the on–off current ratio in logical devices made of G/SnO_2 HTSs would be largely improved. Since the presence of a finite E_g without degrading the electronic properties of graphene is highly expected, SnO_2 is a suitable choice as a substrate for graphene-related electronic devices.

Now, we turn to the bilayer graphene (BLG) on SnO_2 surface. The stacking patterns are simulated by adding another graphene monolayer on patterns TO, TS, and

RSC Advances Accepted Manuscript

B of G/SnO_2 HTSs, which are still defined as patterns BTO, BTS, and BB, respectively. In all the cases, the BLG is arranged in two different ways, i.e., AA and AB (Bernal stacking order). After structural relaxation, we find that the AB stacking order of graphene is more stable energetically than AA order. and thus we only considering pattern AB in the following, as shown in Figs. 5(a-c). The optimized interlayer spacing between BLG and SnO_2 interface preserves about 3.6 Å, consistent with monolayer graphene on SnO_2 surface. The relaxed interlayer spacing between graphene sheets is found to be larger than the typical length of C-C bond (1.42 Å) in monolayer graphene, suggesting that the bonds in BLG are absent in all the hybrid structures.

Fig. 6 displays the electronic band structures of BLG on SnO_2 substrate in the ground state AB. It can be seen that around the Fermi level, the band structures of G/SnO_2 HTSs have the characteristic graphene feature of linear dispersions, i.e., the merits of Dirac system, such as the high Fermi velocity and large carrier mobility, may be well retained in the G/SnO_2 HTSs. More importantly, these stacking patterns exhibit the semiconducting character with an energy-gap of 110 meV, larger than k_BT (26 meV) at room temperature, differ from the previous report on BLG on semiconductors.

In generally, to realize the practical applications of G/SnO_2 HTSs in FET, higher carrier mobility and linear band dispersion are very essential. So we investigate the electron effective mass (m*) at Dirac point of G/SnO_2 HTSs. As have mentioned before, the G/SnO_2 HTSs preserve the linear band dispersion relation of graphene. According to the graphene dispersion relationship, the m_e* and m_h* can be expressed as [39-41]

$$m^* \approx \frac{p}{v_g} \approx \frac{\hbar k}{v_f} \qquad (3)$$

where k is wave vector and v_f is Fermi velocity. Table II present the calculated fitting

RSC Advances Accepted Manuscript

value of v_f for all G/SnO_2 HTSs. Fortunately, it can be seen that all the stacking patterns obtain a considerable v_f value (~0.81×10^6 m/s), which is comparable to that of FSG (1.0×10^6 m/s). Furthermore, we also investigate the calculated m_e* and m_h* along Γ-K and K-M directions of all the stacking patterns, as shown in Table II. It can be observed that the m_e* and m_h* at VBM and CBM for G/SnO_2 HTSs are very small, which is still more superior to others graphene-based nanoelectronics. This indicates that the G/SnO_2 HTSs may have a higher carrier mobility which is necessary in the application of FETs. The large value of v_f and the less m* is indispensable for the design of application and this can be analyzed qualitatively by the interaction between graphene and SnO_2 substrate. Similar results are also found for BLG/SnO_2 HTSs. As a consequence, an ideal FET with the high carrier mobility and certain band gap on G/SnO_2 HTSs based nanoelctronics can be expected.

IV. Conclusions

In summary, our first-principles study indicates that the graphene can grows on SnO_2 substrates with a binding energy of about -67~-70 meV per C atom, irrespective of the adsorption patterns, suggesting vdW interaction between graphene and SnO_2 monolayer. Different from the conventional G/semiconductor HTSs, the Dirac cone of the G/SnO_2 HTS appears yet, but the metallic character of HTSs is obtained. However, the FDG peeled from G/SnO_2 HTS exhibit semiconducting behavior with a sizeable band gaps of 10.2~12.6 meV at K point. When the bilayer graphene is deposited on SnO_2 substrate, however, a global gap of 100 meV is formed at the Fermi level. Also, the nearly linear band dispersion character of graphene can be preserved in all graphene and bilayer graphene on SnO_2 substrate, and thus high carrier mobility of graphene is expected. Our finds provide a better understanding of the interfacial properties of G/SnO_2 HTSs and help to design the high-performance FET in nanoelectronics.

RSC Advances Accepted Manuscript

Acknowledgements: This work was supported by the National Natural Science Foundation of China (Grant No. 11274143, 11434006, 61172028, and 11304121), and Research Fund for the Doctoral Program of University of Jinan (Grant no. XBS1433).

RSC Advances Accepted Manuscript

RSC Advances Accepted Manuscript

References

(1) K. S. Novoselov, A. K. Geim, S. V. Morozov, D. Jiang, Y. Zhang, S. V. Dubonos, I. V. Grigorieva and A. A. Firsov, *Science* 2004, **306**, 666-669.

(2) K. S. Novoselov, A. K. Geim, S. V. Morozov, D. Jiang, M. I. Katsnelson, I. V. Grigorieva, S. V. Dubonos and A. A. Firsov, *Nature* 2005, **438**, 197-200.

(3) Y. W. Son, M. L. Cohen and Louie, S. G. *Nature* 2006, **444**, 347-349.

(4) M. Otani, M, Koshino, Y. Takagi and S. Okada, *Phys. Rev. B.* 2010, **81**, 161403-161406.

(5) J. B. Oostinga, H. B. Heersche, X. Liu, A. F. Morpurgo and L. M. Vandersypen, *Nature Mater.* 2007, **7**, 151-157.

(6) Y. B. Zhang, T. T. Tang, C. Girit, Z. Hao, M. C. Martin, A. Zettl, M. F. Crommie, Y. R. Shen and F. Wang, *Nature* 2009, **459**, 820-823.

(7) Y. Zhang, Y. W.Tan, H. L. Stormer and P. Kim, *Nature* 2005, **438**, 201-204.

(8) S. V. Morozov, K. S. Novoselov, M. I. Katsnelson, F. Schedin, D. C. Elias, J. A. Jaszczak and A. K. Geim, *Phys. Rev. Lett.* 2008, **100**, 016602-016605.

(9) H. Okamoto, Y. Kumai, Y. Sugiyama, T. Mitsuoka, K. Nakanishi, T. Ohta, H.

Nozaki, S. Yamaguchi and S. Shirai, et al. *J. Am. Chem. Soc.* 2010, **132**, 2710-2718.

(10) L. Jiao, L. Zhang, X. Wang, G. Diankov and H. Dai, *Nature* 2009, **458**, 877-880.

(11) R. Bog, B. Jørgensen, L. Nilsson, M. Andersen, E. Rienks, M. Bianchi, M. Fanetti, E. Lægsgaard, A. Baraldi, S. Lizzit, Z. Sljivancanin, F. Besenbacher, B. Hammer, T. G. Pedersen, P. Hofmann and L. Homekaer, *Nat. Mater.* 2010, **9**, 315-319.

(12) F. Guinea, M. I. Katsnelson and Geim, A. K. *Nat. Phys.* 2010, **6**, 30-33.

(13) W. J. Zhang, C. T. Lin, K. K. Liu, T. Tite, C. Y. Su, C. H. Chang, Y. H. Lee, C. W. Chu, K. H. Wei, J. L. Kuo and L. J. Li, *ACS Nano.* 2011, **9**, 7517-7524.

(14) S. Y. Zhou, G. H. Gweon, A. V. Fedorov, P. N. First, W. A. Heer, D. H. Lee, F. Guinea, A. H. Castro Neto and A. Lanzara, *Nat. Mater.* 2007, **6**, 770-775.

(15) E. Rollings, G. H. Gweon, S. Y. Zhou, B. S. Mun, J. L. McChesney, B. S. Hussian, A. V. Fedorov, P. N. First, W. A. DeHeer and A. Lanzara, *J. Phys. Chem. Solids* 2006, **67**, 2172-2177.

(16) Y. Ding and Y. Wang, *Appl. Phys. Lett.* 2013, **100**, 083102-083105.

(17) Y. D. Ma, Y. Dai, W. Wei, C. W. Niu, L. Yu and B. B. Huang, *J. Phys. Chem. C* 2011, **115**, 20237-20241.

(18) H. Kim, S. W. Kim, Y. U. Park, H. Gwon, D. H. Seo, Y. Kim and K. Kang, *Nano Res.* 2010, **3**, 813-821.

(19) S. J. Ding, D. Luan, F. Y. Boey, J. S. Chen and X. W. Lou, *Chem. Commun.* 2011, **47**, 7155-7157.

(20) L. Miao, J. B. Wu, J. J. Jiang, and P. Liang, *J. Phys. Chem. C* 2013, **117**, 23-27.

(21) S. M. Paek, E. Yoo and I. Honma, *Nano Lett.* 2009, **9**, 72-75.

RSC Advances Accepted Manuscript

(22) G. Kresse and J. Furthmuller, *Phys. Rev. B.* 1996, **54**, 11169-11186.

(23) G. Kresse and J. Hafner, *Phys. Rev. B.* 1994, **49**, 14251-14269.

(24) G. Kresse and D. Joubert, *Phys. Rev. B.* 1999, **59**, 1758-1775.

(25) J. P. Perdew, K. Burke and M. Ernzerhof, *Phys. Rev. Lett.* 1996, **77**, 3865-3868.

(26) S. Grimme, *Journal of computational chemistry* 2006, **27(15)**, 1787-1799.

(27) T. Bučko, J. Hafner, S. Lebègue and J. G.Ángyán, *J. Phys. Chem. A* 2010, **114**, 11814-11824.

(28) L. Magaud, F. Hiebel, F. Varchon, P. Mallet and J. Y. Veuillen, *Phys. Rev. B.* 2009, **79**, 161405-161408.

(29) K. Kamiya, N. Umezawa and S. Okada, *Phys. Rev. B.* 2011, **83(15)**, 153413-153416.

(30) H. X. Luan, C. W. Zhang, F. Li, P. Li and P. J.Wang, *RSC Advances* 2014, **4**, 9602-9607.

(31) S. S. Li, C. W. Zhang, W. X. Ji, F. Li and P. J. Wang, *Phys. Chem. Chem. Phys.* 2014, **16(41)**, 22861-22866.

(32) J. B. Oostinga, H. B. Heersche, X. Liu, A. F. Morpurgo and L. M. Vandersypen, *Nat. Mater.* 2007, **7(2)**, 151-157.

(33) Y. Fan, M. Zhao, Z. Wang, X. Zhang and H. Zhang, *Appl. Phys. Lett.* 2011, **98**, 083103-083105.

(34) S. Kokott, P. Pflugradt, L. Matthes and F. Bechstedt, *J. Phys.:Condens. Matter* 2014, **26**, 185002-185005.

(35) S. Cahangirov, M. Topsakal, E. Akturk, H. Sahin and S. Ciraci, *Phys. Rev. Lett.* 2009, **102**, 236804-236807.

(36) C. W. Zhang and S. S. Yan, *J. Phys. Chem. C* 2012, **116**, 4163-4166.

(37) N. T. Cuong, M. Otani and S. Okada, *Phys. Rev. Lett.* 2011, **106(10)**,

RSC Advances Accepted Manuscript

106801-106804.

(38) G. Giovannetti, P. A. Khomyakov, G. Brocks, P. J. Kelly, J. van den Brink, *Phys. Rev. B.* 2007, **76**, 073103-073106.

(39) K. S. Novoselov, A. K. Geim, S. V. Morozov, D. Jiang, M. I. Katsnelson, I. V. Grigorieva, S. V. Dubonos and A. A. Firsov, *Nature* 2005, **438,** 197-200.

(40) P. Avouris, Z. H. Chen and V. Perebeinos, *Nature nanotechnology* 2007, **2**, 605-615.

(41) A. H. Castro Neto, F. Guinea, N. M. R. Peres, K. S. Novoselov and A. K. Geim, *Rev. Mod. Phys*. 2009, **81**, 109-162.

RSC Advances Accepted Manuscript

Table I The calculated distance between graphene and SnO_2 monolayer, and the binding energy (meV/C atom) of graphene on different adsorption sites with DFT and DFT-D2, respectively.

Table II The calculated effective masses of electrons and holes, the maximum Fermi velocity (v_f) for all stacking patterns of G/SnO_2 HTSs.

Fig. 1 Side and top views of the three patterns of G/SnO_2 HTS: (a) TO, (b) TS, and (c) B; as well as (d) FDG of pattern B. The blue, red and green balls represent C, O and Sn atoms, respectively.

Fig. 2 Binding energy (E_b) per C atom in G/SnO_2 HTSs for the three patterns TO, TS, and B, respectively, as a function of the spacing between the graphene and SnO_2 monolayer. The insert is the enlarged plot near the equilibrium lattice of G/SnO_2 HTSs.

Fig. 3 Band structures of the G/SnO_2 HTS for patterns (a) TO, (b) TS, (c) B, (d) SnO_2 monolayer, and (e) free-standing graphene. (f) is PDOS of pattern TO in the ground

RSC Advances Accepted Manuscript

state.

Fig. 4 (a) The differential charge density (0.005 e/Å^3) of pattern B. Here, the yellow (cyan) indicates the charge accumulation (depletion). (b) Plane-averaged electron density difference, $\Delta\rho$ (z) for pattern B. The q is the charge transfer calculated by integrating $\Delta\rho$ (z) over the full z range. The yellow and cyan areas represent electron accumulation and depletion, respectively.

Fig. 5 Band structures of the FDG in patterns (a) TO, (b) TS, (c) B, respectively. The insert is the enlarged band gap at the Fermi level. The Femi level points to zero energy.

Fig. 6 Side and top views of the three patterns of BLG/SnO_2 HTS: (a, d) TO, (b, e) TS, and (c, f) B. The blue, red and green balls represent C, O and Sn atoms, respectively.

Fig. 7 Band structures for BLG/SnO_2 HTSs in patterns (a) BTO, (b) BTS, (c) BB, respectively. The insert is the enlarged band gap at the Fermi level.

RSC Advances Accepted Manuscript

Table I The calculated distance between graphene and SnO_2 monolayer, and the binding energy (meV/C atom) of graphene on different adsorption sites with DFT and DFT-D2, respectively.

Patterns	DFT(without vdW)		DFT-D2(with vdW)	
	d (Å)	E_b (meV)	*d* (Å)	E_b (meV)
TO	3.59	-11.67	3.07	-67.23
TS	3.61	-11.34	3.07	-67.22
B	3.67	-16.56	3.11	-70.42

RSC Advances Accepted Manuscript

Table II The calculated effective masses of electrons and holes, the maximum Fermi velocity (v_f) for all stacking patterns of G/SnO_2 HTSs.

Patterns	Effective mass	Γ-K	Γ-M	V_f (max)
TO	m_e*	6.78×10^{-19}	6.14×10^{-19}	0.80×10^{6}
	m_h*	6.98×10^{-19}	6.78×10^{-19}	
TS	m_e*	6.58×10^{-19}	6.32×10^{-19}	0.80×10^{6}
	m_h*	6.97×10^{-19}	6.43×10^{-19}	
B	m_e*	6.42×10^{-19}	6.38×10^{-19}	0.81×10^{6}
	m_h*	6.99×10^{-19}	6.56×10^{-19}	

RSC Advances Accepted Manuscript

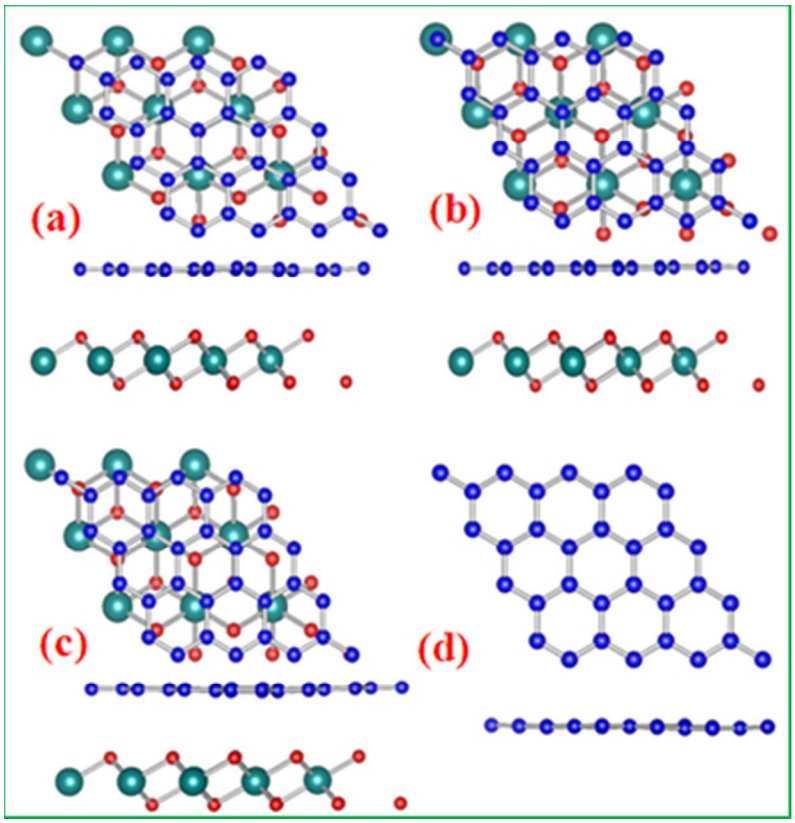

103x107mm (96 x 96 DPI)

RSC Advances Accepted Manuscript

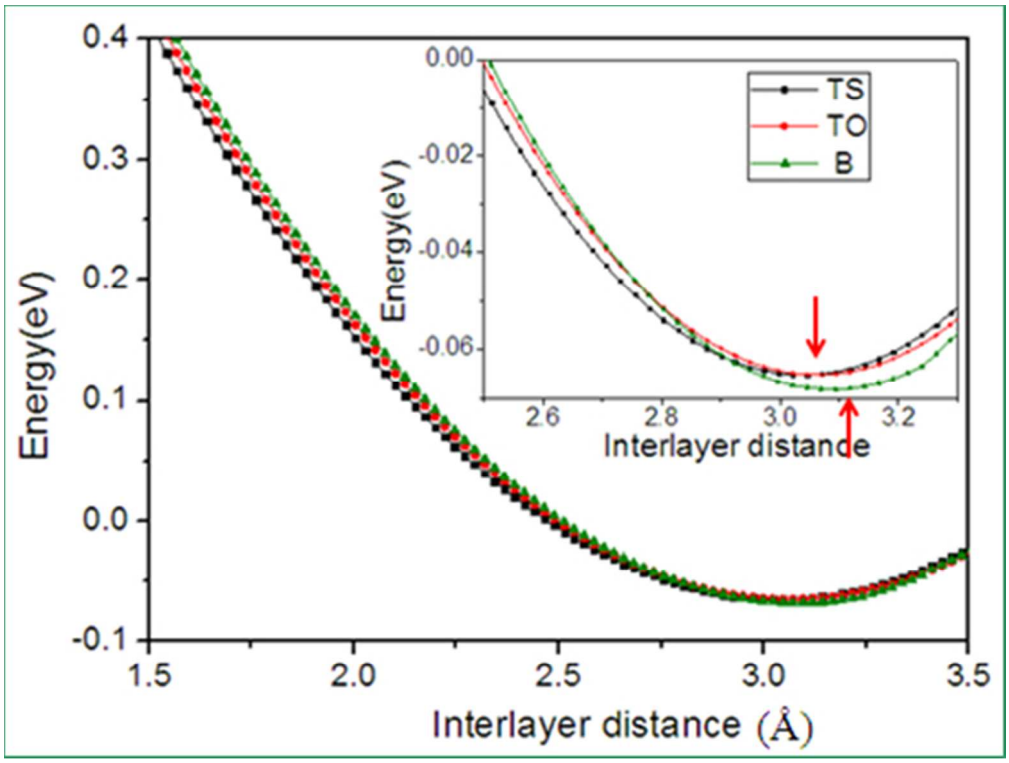

144x108mm (96 x 96 DPI)

RSC Advances Accepted Manuscript

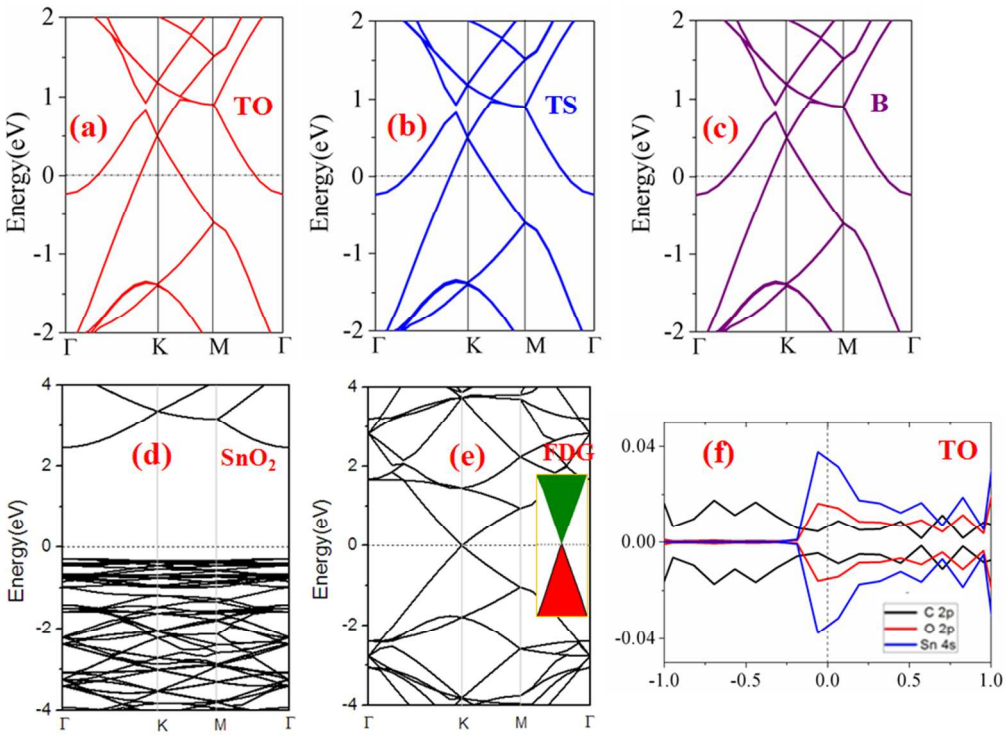

255x186mm (96 x 96 DPI)

RSC Advances Accepted Manuscript

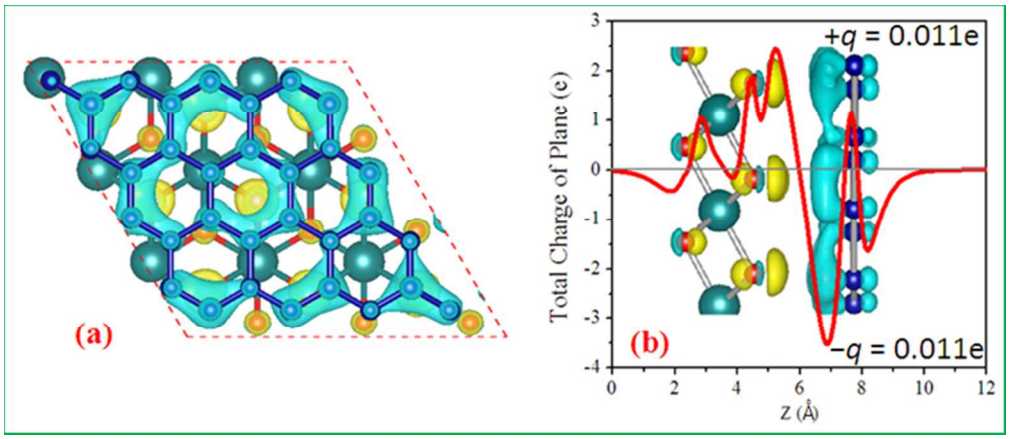

196x84mm (96 x 96 DPI)

RSC Advances Accepted Manuscript

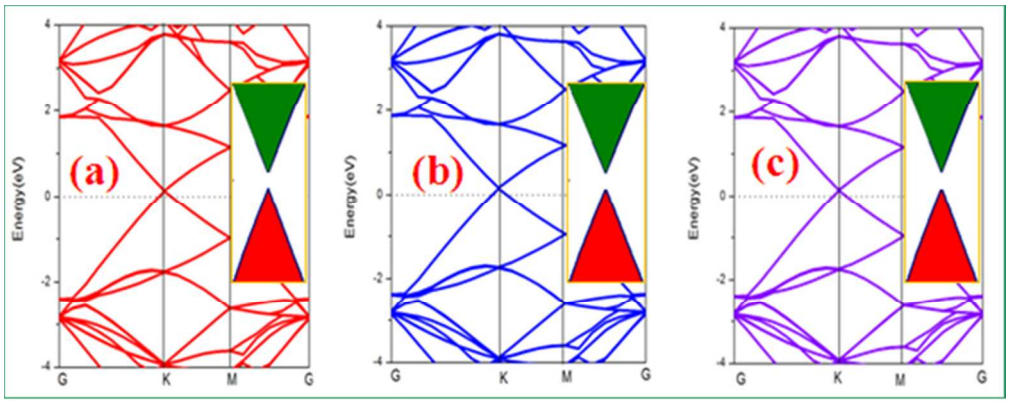

196x77mm (96 x 96 DPI)

RSC Advances Accepted Manuscript

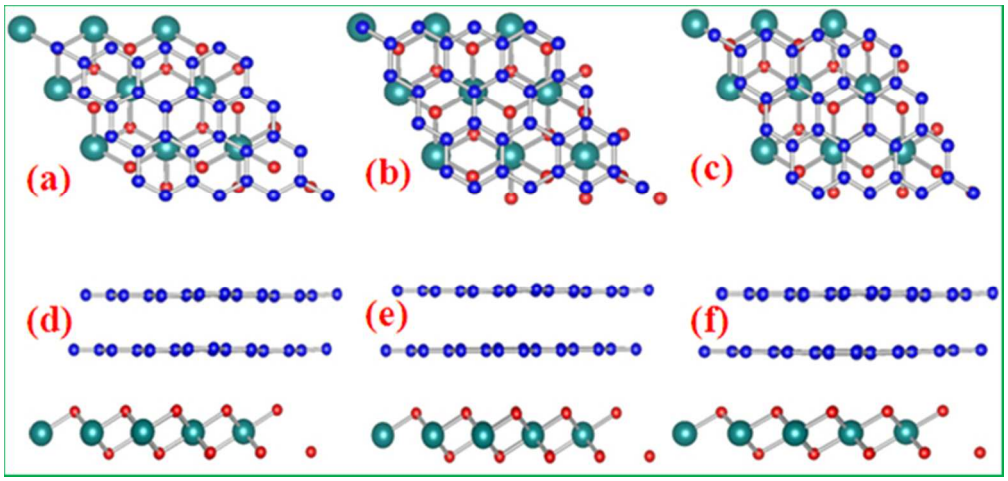

177x83mm (96 x 96 DPI)

RSC Advances Accepted Manuscript

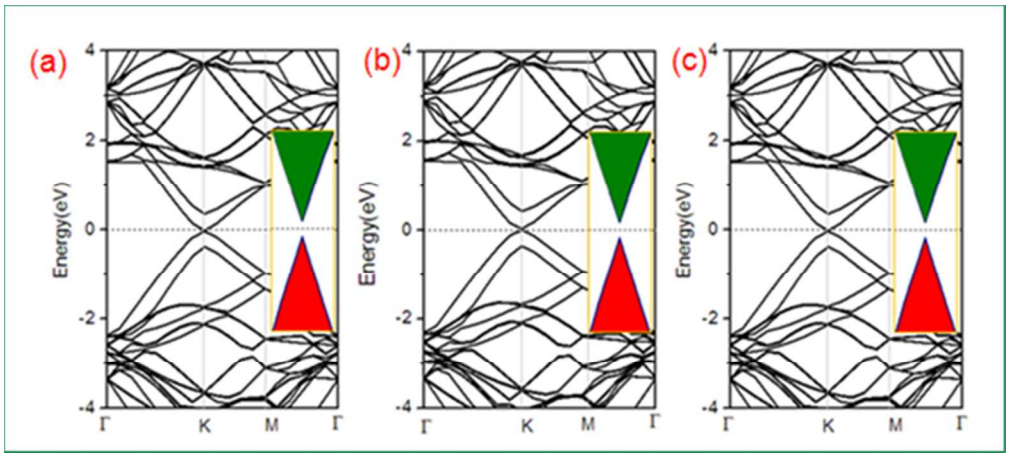

175x78mm (96 x 96 DPI)

RSC Advances Accepted Manuscript